Transportation Geotechnics 52 (2025) 101581

Contents lists available at ScienceDirect

Transportation Geotechnics

journal homepage: www.elsevier.com/locate/trgeo

Original Article

Novel method to estimate the stiffness of compacted granular geomaterials

Samuel Valencia-Díaz [a], Jacob D.R. Bordón [b], J. Yepes [c], Juan J. Aznárez [b], Miguel A. Franesqui [d,*]

[a] Departamento de Ingeniería Civil, Universidad de Las Palmas de Gran Canaria (ULPGC), Campus de Tafira, 35017 Las Palmas de Gran Canaria, Spain
[b] Instituto Universitario de Sistemas Inteligentes y Aplicaciones Numéricas en Ingeniería, Universidad de Las Palmas de Gran Canaria (ULPGC), Campus de Tafira, 35017 Las Palmas de Gran Canaria, Spain
[c] Departamento de Ingeniería Civil – IOCAG, Universidad de Las Palmas de Gran Canaria (ULPGC), Campus de Tafira, 35017 Las Palmas de Gran Canaria, Spain
[d] Grupo de Fabricación Integrada y Avanzada – Departamento de Ingeniería Civil, Universidad de Las Palmas de Gran Canaria (ULPGC), Campus de Tafira, 35017 Las Palmas de Gran Canaria, Spain

ARTICLE INFO

Keywords:
Soil strain modulus
Soil stiffness test
miniature plate load test (mPLT)
Compacted fill
Subgrade design
Granular base
Pavement design

ABSTRACT

Transport infrastructure involves the use of large volumes of compacted geomaterials, leading to significant economic and environmental impacts that need to be addressed in all stages of the project. A new laboratory procedure to estimate the stiffness of embankments, subgrades, granular bases and subbases is proposed. The utilization of well-established and simple equipment results in an easy-to-conduct and cost-effective method that combines the compaction procedure of a Modified Proctor test with the loading scheme of a repetitive static plate load test, adapted to the reduced geometry of this new 'miniature plate load test' (mPLT). This enables the estimation of the compaction characteristics and the vertical strain modulus in a single test. Subsequently, the elastic modulus needed for analytical design is derived through back-calculation using a numerical model. Soil specimens were tested using different gradations, compaction energies and moisture contents to generate various regression surfaces that correlate the variables of interest. Furthermore, the laboratory strain modulus obtained from this test was compared with full-scale static plate load tests conducted in the field. The results show that this methodology could become a valuable reference test to aid in the design and quality control of compacted fills for civil infrastructures.

Introduction

Transport infrastructure involves the use of large volumes of compacted geomaterials for the construction of embankments, subgrades, and granular bases and subbases of pavements that represent a substantial part of the total project cost. If the terrain is rugged, they can account for up to 40 % of the necessary investment [1], in addition to leading significant environmental impact. These issues need to be addressed in all stages of the project, especially through design optimization, for which it is necessary to make accurate predictions of the mechanical properties of the geomaterials.

The practice of pavement and subgrade design is based on both engineering principles (analytical component) and experience (empirical component). Thus, current trend is the use of the so-called Mechanistic-Empirical approach, where pavement response (i.e. stresses, strains and deflections) is calculated analytically and the mechanical properties and failure conditions of the materials are obtained experimentally. Pavement design is a complex iterative process in which solid connections between design, construction and service stages are required.

During the design stage, different models can be used to determine pavement response in the mechanistic analysis. It is well known that most pavement materials are heterogeneous, present several levels of anisotropy and exhibit non-linear behaviour, including the viscoelastic performance of bituminous materials and the influence of moisture conditions on the subgrade response. However, it is still common practice to model flexible pavements as elastic layered systems with infinite lateral dimensions including the subgrade, which can be formed itself by different layers of soils (natural and/or stabilized) where the deepest is treated as an infinite half-space following Boussinesq's theory. Despite its shortcomings, the use of elasticity theory adequately simulates the global behaviour of compacted granular geomaterials subjected to limited stresses and strains (i.e. resilient response), which significantly simplifies the calculation process and resources [2,3].

The linear-elastic model requires two elastic constants as input

* Corresponding author.
E-mail address: miguel.franesqui@ulpgc.es (M.A. Franesqui).

https://doi.org/10.1016/j.trgeo.2025.101581
Received 18 February 2025; Received in revised form 28 April 2025; Accepted 4 May 2025
Available online 6 May 2025

parameters for analytical design, typically Young's modulus (E) and Poisson's ratio (ν). However, the prediction of such soil elastic properties is a formidable task due to not only the many variables involved, most of them unknown at design stage, but also to the existence of interrelations and coupling effects between them. In addition to this, compacted fills and embankments are normally in a partially saturated state, (i.e. unsaturated soil mechanics principles) further increasing the complexity of said predictions. Although this topic has been subject to controversy [4], it is generally accepted that field stress–strain soil states due to traffic loading are best simulated using cyclic triaxial laboratory tests. Current M−E Pavement Design Guide [5] uses the resilient modulus (M_R) as an input in analytical design. Its related laboratory test arose to bridge the gap between theory and experience after the AASHO Road Test [6], but although some improvements have been made [7], this test is still relatively time-consuming and difficult to conduct.

In the construction stage the methods to control the level of compaction, bearing capacity and stiffness of compacted fills are well regulated by technical specifications, following procedures based on laboratory and field testing. In the laboratory, the California Bearing Ratio (CBR) test is one of the most widely used. This test was introduced in 1929 to overcome some of the difficulties of field loading tests, providing a simple and rapid method for comparing the bearing capacity of compacted geomaterials [8]. The importance of density and its relations with soil type, compaction energy and moisture content in earthwork construction can be traced back to the first studies on soil compaction carried out by Ref. [9–11]. Recently, further significant developments such as intelligent compaction technologies have come into scene to enhance quality and uniformity [12].

From a compaction quality assurance perspective, the so-called density-based methods have traditionally been used although modulus-based methods have also been implemented in most transportation agencies specifications. The existence of both methods is explained by the fact that satisfying density and moisture content criterion on its own does not necessarily imply adequate stiffness and, conversely, meeting stiffness criterion alone does not guarantee the long-term stability of the construction [13,14]. Consequently, suitable in-place density and moisture content, or more appropriately degree of saturation [15,16], along with sufficient stiffness are of paramount importance in the behaviour of compacted geomaterials used in transport infrastructure.

Thus, it is of practical interest to develop new methods that allow the evaluation of the relations between the stiffness properties and the soil state variables. Moreover, stiffness characteristics are important not only from a compaction quality perspective but also from a design point of view, as they allow for the prediction of the elastic modulus used in the mechanistic design. Different studies have been carried out to evaluate the relationship between strain modulus and its influencing factors, which can be broadly divided into state and loading factors. Focusing on the state factors, a highly significant effect of moisture content on the strain modulus has been demonstrated. Conversely, a solid correlation between strain modulus and dry density has not been confirmed, which it is thought to be a consequence of the complex interaction among dry density, moisture content, and degree of saturation in partially saturated compacted fills [13]. It is known that for a given soil there is not a unique value of strain modulus as it depends on the state conditions for which it is determined [17]. This leaves the door open for the development of new procedures to estimate the elastic moduli of compacted geomaterials required in analytical design that can accurately simulate the stress–strain performance during the service life of the infrastructure.

In this context, bearing plate devices have been used since the very beginning in pavement research [18,19] and their use for quality assessment of compacted geomaterials (i.e. modulus-based control) is widely spread. There are different variants of field plate load tests (PLT) which can be grouped in static and dynamic, and non-repetitive and repetitive tests depending upon the nature of the loading and the number of loading cycles applied, respectively. Repetitive static PLT is standardised in many countries for compaction control [20–22]. Secant vertical strain moduli (E_v) in both a first and a second loading cycle are calculated from the stress-settlement curve. The second cycle strain modulus (i.e. reloaded modulus) along with the ratio between the second and first cycle moduli (E_{v2} / E_{v1}) are used as compaction control parameters by many transportation agencies.

PLT can also be used for the estimation of the elastic modulus of pavement components required in design through back calculation process [23]. The analytical formula derived from the theory of elasticity for the determination of the theoretical settlement under a circular loaded area can be used for trial determinations of the 'surface modulus' (also called 'equivalent modulus') of layered systems.

However, both the static field PLT and the cyclic triaxial laboratory test previously mentioned, are time-consuming and costly. The former (*in situ* test) cannot usually be performed at the design stage. The latter requires complex equipment and is difficult to conduct for purely granular soils due the absence of cohesion, which is relevant because granular soils are the more frequently used for subgrades, subbases and bases of pavements.

Due to the extensive experience accumulated with the CBR test, many studies have attempted to establish empirical correlations between the CBR index, a bearing capacity parameter, and different properties related to material stiffness. Some of them have been widely used [24–26]. Several studies have shown that there is no unique relationship between the Young's modulus and CBR due to the influence of the deviator stress [27]. A recent study has compiled the many correlations between the resilient modulus and the CBR index proposed for different soil types around the world [28]. This shows that there is no universal correlation between modulus and CBR, but that it must be obtained specifically for each soil type and even for certain soil state conditions. Despite its well-known limitations, the CBR test is still widely used to characterize the materials and to correlate with the stiffness of the subgrade at the design stage by certain agencies [29]. In this line, some authors have proposed using the laboratory CBR test to predict the resilient modulus from the stress–strain curve under elasto-plastic behaviour before failure with the aid of elastic numerical models simulating the test [30]. Others have also suggested determining the elastic modulus by searching relationships between the CBR and static plate load tests [31–36]. However, interpreting the PLT results for unsaturated soils remains problematic due to the influence of suction [37], and the existence of scale effects [38,39].

Consequently, there is a need for further research on simpler, quicker, but sufficiently precise and more affordable empirical procedures to reliably assess the stiffness properties of the geomaterials, which will subsequently allow the optimisation of compacted earthworks analytical design and thus, contribute to improve their quality and reduce their significant cost and environmental impact.

With respect to the analytical part of the design, numerical methods using multilayer models are widely used. The most common is the Finite Element Method (FEM) due to its versatility but it requires the discretization of the entire domain. The Boundary Element Method (BEM) reduces the dimension of the problem by limiting it to the boundary, which it is advantageous for certain problems [40]. Pavement design is based on the theory of infinite-dimensional multilayer masses (i.e. unbounded domains), for which the application of BEM is beneficial [41]. When a Green's Function for an infinite horizontally multilayered half-space [42] is used in the BEM, only the plate-soil interaction needs to be discretised.

In the present study, a methodology to assess the stiffness properties for the optimum design of earthworks (embankments, subgrades, granular bases and subbases) with compacted granular geomaterials in transport infrastructures is proposed. This research covers the following aspects:

a) Development of a new two-stage laboratory test, which combines the same procedure of a Modified Proctor (MP) test with the loading scheme of a repetitive static plate load test, adapted to the reduced geometry of this new 'miniature plate load test' (mPLT). This way, not only moisture content – dry density couples but also their corresponding secant vertical strain moduli are obtained.
b) Laboratory testing of extensive series of soil specimens using different gradations, compaction energies and moisture contents, as the first step to validate the proposed methodology.
c) Study of relations between stiffness indexes and soil state properties based on the empirical results.
d) Geometrical representation of the results in a 3D–space (moisture content – dry density – strain modulus) using non-linear regression surfaces to facilitate the analysis of the phenomenon and allow for strain modulus estimation and correlation for different state conditions.
e) Derivation of the Young's modulus required for analytical design from the laboratory modulus through back-calculation with the aid of numerical modelling.
f) Preliminary correlation between the strain modulus provided by this new laboratory test and field static PLT modulus.

Methodology

Materials and laboratory testing

This study was based on soil samples taken from a construction site located in the north-west of the island of Gran Canaria, Canary Islands (Spain). Geologically, this material consists of olivine-pyroxene basalt and plagioclase lavas (B-OP-M), with subordinate trachybasalt (TB). A detailed classification for construction applications of volcanic geomaterials was proposed by Ref. [43], showing that they can be characterized using commonly used geotechnical methods and tests.

Four soil gradations were produced with the geomaterial mentioned above, namely NAT20, SEL20, TOL20 and NAT10, where the number indicates the maximum particle size (mm). Thus, most of soil gradations were limited to sieve #20 mm as usual in Modified Proctor (MP) and CBR tests. Gradations labelled with 'NAT' represent the natural soil obtained directly from site. 'SEL' and 'TOL' were modified gradations that reproduce the so-called 'select' and 'tolerable' soil gradations, according to the soil classification system of the Spanish specifications [44], to simulate different soil types frequently encountered in compacted fills. Most tests in this work used soil gradation NAT20 (Fig. 1a) and its laboratory results were used to correlate with field results. The main characteristics of the different soil gradations according to European standards are shown in Table 1. The grading curves are shown in Fig. A1 (Appendix 1).

Table 1
Main characteristics of the geomaterials tested.

Characterization property		Soil gradation			
		NAT20	TOL20	SEL20	NAT10
Gradation [EN ISO 17892–4]	#20 (mm)	100	100	100	100
	#10 (mm)	85.17	95	70	100
	#4 (mm)	59.61	85	42	70.73
	#2 (mm)	43.27	81	28.5	50.68
	#0.5 (mm)	13.62	40.5	15	17.32
	#0.08 (mm)	5.96	5.96	5.96	5.96
Uniformity	Cu	19.1	10	36.8	18.7
Curvature	Cc	1.7	0.78	3.6	1.7
Specific Gravity [EN ISO 17892–3]	Gs	2.85	2.85	2.85	2.85
Plasticity [EN ISO 17892–12]	LL	30.6	30.6	30.6	30.6
	PL	26.8	26.8	26.8	26.8
	PI	3.8	3.8	3.8	3.8
Compaction [EN 13286–2]	OMC (%)	9	10.3	8.5	–
	MDD (g/cm^3)	2.22	2.1	2.2	–
Bearing Capacity [EN 13286–47]	CBR (100 % MP)	66	62	67	–
Chemicals [CEN / TS 17685–2]	OM (%)	0.23	0.23	0.23	0.23
[UNE 103205:2019]	SS (%)	0.31	0.31	0.31	0.31
Soil Classification	USCS	SW-SM	SP-SM	GP-GM	SW-SM
	AASHTO (USA)	A-1-a	A-2–4	A-1-a	A-2–4
	PG-3 (Spain)	ADE	TOL	ADE	ADE

(NAT) Natural soil; (TOL) Tolerable soil type; (SEL) Select soil type; (ADE) Adequate soil type; (Cu) Coefficient of uniformity; (Cc) Coefficient of curvature; (Gs) Specific gravity of solid particles (related to water density); (LL) Liquid limit; (PL) Plastic limit; (PI) Plasticity index; (MP) Modified Proctor; (OMC) MP Optimum moisture content; (MDD) MP Maximum dry density; (OM) Organic matter; (SS) Soluble salts.

Multiple soil specimens were prepared for each of the four soil gradations allowing to conduct a series of 92 'miniature plate load tests' (mPLT). These tests were grouped as follows: 66 NAT20, 8 NAT10, 9 TOL20 and 9 SEL20. This new laboratory test procedure consists of a small-scale version of the standard in-situ static plate load test (PLT) but using laboratory equipment commonly used in geotechnical practice. This procedure may be viewed as an extension of a Modified Proctor (MP) compaction test where a loading stage like the repetitive PLT is

Fig. 1. Laboratory miniature plate load tests (mPLT): (a) Soil fractions (gradation NAT20); (b) Compacted soil specimen under loading process; (c) Compacted soil specimen demoulded just after loading.

added.

The minimum number of specimens per compaction energy for soil gradation NAT20 was determined based on a 95 % confidence level assuming a standard deviation for the second cycle modulus of 50 MPa within a group (i.e. same compaction effort) and a maximum margin of error of 10 MPa. This assumption was later checked with calculated standard deviations.

The mPLT test was divided into two stages, namely compaction stage and loading stage. In the first stage, soil specimens were compacted following the same procedure of a MP test but at varying compaction energies (25, 50, 75, 100 and 125 % with respect to the MP test) and moisture contents (2 % to 12 %). These were selected to cover a wide range of state conditions (i.e. dry density and moisture content), from normal to extreme. Specimens were compacted using CBR moulds with spacer discs ($\varnothing_{mould}$ = 152.5 mm). Discounting the height of the spacer disc, the specimen height is 127 mm. In the second stage, each soil specimen was loaded using a CBR piston ($\varnothing_{piston}$ = 50 mm) but without any surcharge around the piston (Fig. 1b) and following a similar pattern to that utilized in a repetitive static PLT according to Spanish code UNE 103808 which is technically equivalent to DIN 18134 and/or ASTM D1195/D1195M-21 standards.

Because the state properties of each specimen are determined right after the loading stage, it is possible to stablish empirical relationships between moisture content, dry density and strain modulus without any significant alteration in the conditions. It is known that the difference between the moisture content at compaction and during testing influences the modulus result more than the moisture content at the time of compaction [45].

The loading process consists of preloading, first loading cycle, unloading and second loading cycle (reloading). These cycles are in turn divided into steps (seven steps for the first loading cycle, three steps for the unloading and six steps for the second loading cycle). The load was held constant during 60 s in each step. The whole loading process was programmed in an automatic loading machine.

A maximum force of 5.9 kN was applied after a preloading force set between 0.1 and 0.2 kN. These parameters were selected based on the stress values stated in the standardised static PLT for the 300 mm, 600 mm and 762 mm diameter plates, which were extrapolated to the piston diameter (50 mm) using a non-linear regression fitting.

This stress level may be excessive for soil specimens compacted at low energies or highly deformable, so it was necessary to establish a complementary stress-based criterion to adjust the maximum applied stress to facilitate the laboratory procedure. Since a theoretical relationship between the applied stress and the CBR index for different penetration values can be derived from the CBR standard, this same relationship was used to set the criterion which is represented in Fig. 2. Following this criterion, maximum applied forces between 7.9 kN and 12 kN would be necessary to produce penetrations of 2.5 mm and 5 mm respectively (for the CBR values between 60 and 70 of this soil, Table 1).

The first and second loading strain moduli (E_{mPLT1}, E_{mPLT2}) and the k-ratio between them ($k = E_{mPLT2} / E_{mPLT1}$) were calculated in line with current PLT standards (Eq. (1), from the secant lines between 30 and 70 % of the maximum applied stress and their related settlements in each cycle as shown in (Fig. 3). This formula is a simplification derived from the general expression that gives the settlement of a perfectly rigid circular plate subject to a uniform load located at the surface of a homogeneous and isotropic elastic half-space, assuming a certain value for the Poisson's ratio [46].

$$E_{mPLT} = 1.5 \cdot r \cdot \frac{\Delta\sigma}{\Delta s} \quad (1)$$

where: E_{mPLT} = strain modulus from mPLT (MPa); r = plate's radius (mm); $\Delta\sigma$ = stress increment (MPa); Δs = settlement increment (mm).

Soil samples were extracted from each compacted specimen after the loading process (Fig. 1c) for moisture content determination using the oven-dry method (24 h in an oven). Dry density, saturation ratio, and void ratio were derived by using theoretical relationships frequently used in Geotechnics.

Numerical model

The experimental mPLT moduli were calculated using the same equation usually employed for the full-scale PLT [Eq. (1)]. This equation is derived from the well-known Boussinesq's half-space theory. However, the mPLT has an additional confinement effect due to the mould. In order to quantify this effect and stablish relationships for use in the practical application of the present methodology, a numerical model was implemented.

The linear-elastic solver MultiFEBE [47] and the mesh generator Gmsh [48] along with auxiliary Matlab® codes were used. The model uses the boundary element method (BEM), for which only the discretization of the boundaries of the domain was required. This domain represents the soil specimen inside the cylindrical mould (152.5 mm in diameter and 127 mm in height). The loaded area corresponds to the CBR piston (50 mm in diameter). Fig. 4a shows the boundary element mesh together with the boundary conditions assumed as follows: imposed displacement in Z-direction below the CBR piston; traction-free to the top surface; null displacement to the bottom; and a combination of null displacements (X- and Y-directions) and traction (Z-direction) to the side wall. A comparison between friction and frictionless wall may lead to differences from 1.7 up to 12 % depending on the Poisson's ratio. The results of this comparison can be found in Table A.1.2 in Appendix 2.

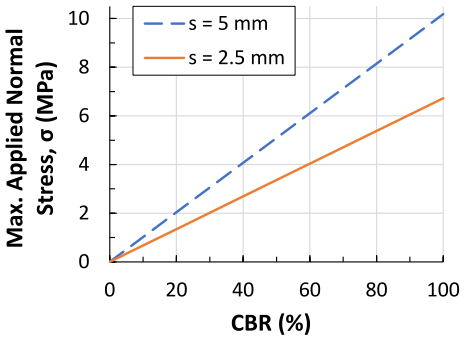

Fig. 2. Applied stress adjustment for mPLT based on CBR test standard.

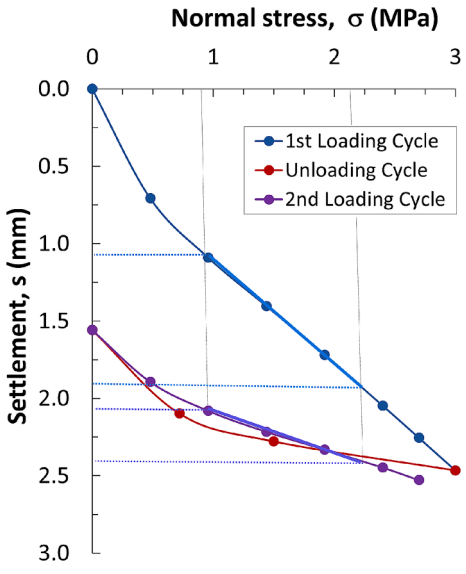

Fig. 3. Calculation of mPLT strain modulus: example of experimental stress-settlement curve.

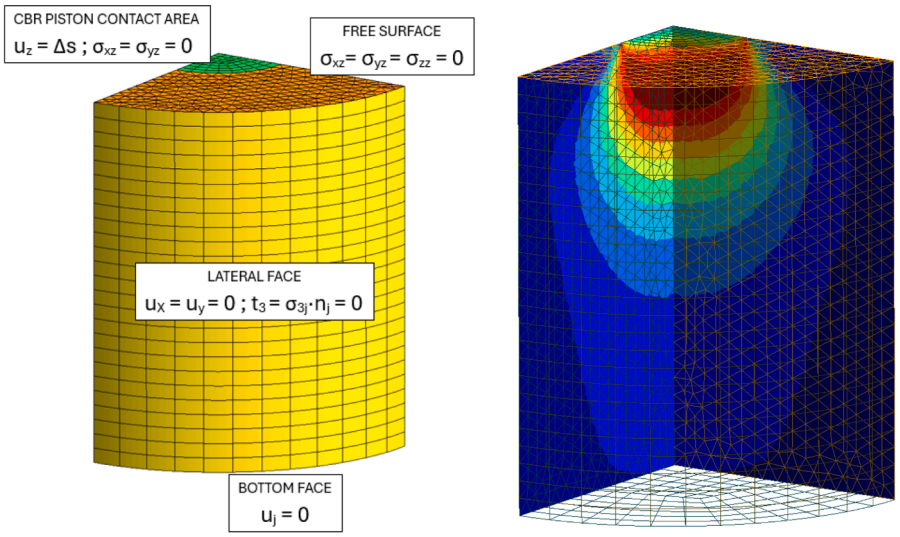

Fig. 4. mPLT numerical model: (a)Boundary mesh (BEM); (b) Simulated bulb of pressure under the loaded area.

The boundary elements were quadratic, and a mesh size of 5 mm was selected. An illustrative example of the bulb of pressure generated below the plate is shown in Fig. 4b.

An analytical relationship between the Young's modulus and the E_{mPLT} modulus was derived numerically, based on the problem of a perfectly rigid plate subject to an imposed vertical displacement. Due to the linear elastic nature of the theoretical model, the following dimensionless group which only depends on the Poisson's ratio can be defined:

$$f(\nu) = \frac{E \cdot \Delta s}{r \cdot \Delta \sigma} \tag{2}$$

The explicit form of this function was obtained by curve fitting, according to the analytical values shown on Table A.1 in Appendix 2, obtaining the following theoretical relationship:

$$E = 1.37 \cdot (1 + 0.325 \cdot \nu - 2.63 \cdot \nu^2) \cdot r \cdot \frac{\Delta \sigma}{\Delta s} \tag{3}$$

which is analogous to that of the well-known half-space problem, but for the confined domain in the mPLT. This also allows relating the E_{mPLT} modulus with the Young's modulus as:

$$E = 0.913 \cdot (1 + 0.325 \cdot \nu - 2.63 \cdot \nu^2) \cdot E_{mPLT} \tag{4}$$

This relationship allows to determine the Young's modulus for use in analytical design (i.e. multilayered elastic model) from the corresponding experimental E_{mPLT} modulus. The Young's modulus needs to be consistent with the Poisson's ratio assumed in design. A graphical representation of this relation for practical applications can be seen in Fig. 10.

Results and discussion

Statistical analysis

An exploratory data analysis was performed to evaluate the quality of the data and whether the tests performed are sufficient from a statistical point of view. Outliers were detected by observing box and whisker plots. Q-Q plots were used to graphically assess data normality to decide whether to use parametric or non-parametric statistical tests. Other assumptions about data distribution were checked when appropriate (e.g. homoscedasticity). Table A.2 in Appendix 3 summarises the main statistics of laboratory tests.

The results of the correlation analysis are shown in Table 2. This type of analysis helps to see whether there is any relation between variables and if so, how strong this relation is. Correlations that are statistically significant have been flagged. Values very close to the unit obey to the existence of known theoretical relations between them. Focusing on factors affecting the strain modulus, the moisture content (MC) is the one that affects the strain modulus the most, among the variables analysed (i.e. Spearman's correlation coefficients show a significant relationship: rho = -0.658, p-value < 0.001). In contrast, the effect of the dry density (DD) does not seem to be so significant.

A Kruskal-Wallis test (i.e. non-parametric version of ANOVA) was performed (Table 3) to study whether there were any significant differences between the means of all the groups (i.e. data grouped by compaction energy [CE] level, expressed as a percent of the energy for a MP test). The main assumptions (independent variable must be categorical, groups should be independent, there should be no significant outliers, data should be approximately normally distributed and there should be homogeneity of variance) were checked. The test showed that CE has a significant effect on the following variables: DD, (e), E_{mPLT1} and E_{mPLT2}. Dunn's post hoc testing revealed that there are significant differences between the following groups: 25–75 (CE, in % with respect to MP test) and 25–100 groups for DD; 25–50, 25–75 and 25–100 for (e); 25–50, 25–75, 25–100 and 50–100 for E_{mPLT1}; 25–75 and 25–100 for E_{mPLT2}.

Relations between stiffness and state properties

Various relationships between variables based on experimental data have been plotted in Fig. 5. In a similar way as stated by Ref. [49] for sandy soils, the dry density (DD) has a general tendency to firstly decrease as the moisture content (MC) increases (for low MC) due to the capillary tension effect (i.e. suction, that inhibits the tendency of the soil particles to move around and be compacted densely). The capillary tension in the pore water has a significant effect on the stiffness of coarse-grained soil [50]. After this first decrease, the DD then increases to a maximum value with further increase of MC, dropping again beyond the OMC (Fig. 5a).

Apparent correlations between the MC (Fig. 5c), or the saturation ratio (S_r) (Fig. 5d), and the second loading cycle strain modulus (E_{mPLT2}) are observable. Although experimental points grouped by fixed CE are not in the same plane either, there is a stronger influence on the stiffness due to the MC or the S_r than due to the dry density (DD), as shown by the

Table 2
Correlation matrix among the different properties.

Variable	MC (%)	DD (g/cm^3)	S_r (%)	e	E_{mPLT1} (MPa)	E_{mPLT2} (MPa)	$k = (E_{mPLT2} / E_{mPLT1})$	Δs_1 (mm)	Δs_2 (mm)
MC (%)	—								
DD (g/cm^3)	0.602***	—							
S_r (%)	0.945***	0.805***	—						
e	−0.600***	−0.999***	−0.805***	—					
E_{mPLT1} (MPa)	0.056	0.401**	0.174	−0.408***	—				
E_{mPLT2} (MPa)	−0.658***	−0.229	−0.574***	0.226	0.446***	—			
$k = E_{mPLT2} / E_{mPLT1}$	−0.251*	−0.519***	−0.369**	0.526***	−0.954***	−0.209	—		
Δs_1 (mm)	−0.057	−0.402***	−0.175	0.409***	−1.000***	−0.446***	0.954***	—	
Δs_2 (mm)	0.662***	0.229	0.577***	−0.226***	−0.463***	−0.996***	0.224	0.462	—

(MC) Moisture content; (DD) Dry density; (S_r) Saturation ratio; (e) Void ratio; (E_{mPLT1}) First loading cycle secant strain modulus from mPLT; (E_{mPLT2}) Second loading cycle secant strain modulus from mPLT; (Δs_1) First loading cycle settlement increment; (Δs_2) Second loading cycle settlement increment.
Levels of significance: (*) $p < 0.05$; (**) $p < 0.01$; (***) $p < 0.001$.

Table 3
Kruskal-Wallis test results.

Variable	Kruskal-Wallis Test	Dunn's post hoc comparisons				
	p-value	CE (% related to MP test)	z	W_i	W_j	p-value
DD (g/cm^3)	<0.001	100—75	1.584	40.219	30.607	0.113
		100—50	1.754	40.219	29.571	0.079
		100—25	4.421	40.219	12.846	< 0.001***
		75—50	0.165	30.607	29.571	0.869
		75—25	2.781	30.607	12.846	0.005**
		50—25	2.619	29.571	12.846	0.009**
E_{mPLT1} (MPa)	<0.001	100—75	0.920	38.875	33.286	0.357
		100—50	1.661	38.875	28.786	0.097
		100—25	4.262	38.875	12.462	< 0.001***
		75—50	0.717	33.286	28.786	0.473
		75—25	3.257	33.286	12.462	0.001**
		50—25	2.554	28.786	12.462	0.011*
E_{mPLT2} (MPa)	0.068	100—75	−0.146	33.688	34.571	0.884
		100—50	1.166	33.688	26.607	0.244
		100—25	2.240	33.688	19.808	0.025*
		75—50	1.270	34.571	26.607	0.204
		75—25	2.309	34.571	19.808	0.021*
		50—25	1.064	26.607	19.808	0.288
$k = (E_{mPLT2} / E_{mPLT1})$	<0.001	100—75	−1.100	19.250	25.929	0.272
		100—50	−1.582	19.250	28.857	0.114
		100—25	−4.068	19.250	44.462	< 0.001***
		75—50	−0.467	25.929	28.857	0.641
		75—25	−2.899	25.929	44.462	0.004**
		50—25	−2.441	28.857	44.462	0.015

(z, W_i, W_j) Dunn's post hoc comparison statistics; (DD) Dry density; (E_{mPLT1}) First loading cycle secant strain modulus from mPLT; (E_{mPLT2}) Second loading cycle secant strain modulus from mPLT.
Levels of significance: (*) $p < 0.05$; (**) $p < 0.01$; (***) $p < 0.001$.

correlation matrix in Table 2. Apparent parabolic trends are observable, which may be explained by the suction effect (an increase in S_r or MC will typically decrease the matrix suction, and hence the modulus, but the same effect is observable if S_r or MC are excessively low). Moreover, when the MC is well below the optimum, the compacted soil structure is extremely sensitive to collapse and thus, a drop in stiffness.

On the contrary, the relation between DD or void ratio (e) and E_{mPLT2} does not show a clear pattern (Fig. 5b and Fig. 5e), which is possibly due to the coupling effects with other variables [45]. In the DD – E_{mPLT2} plane it must be understood that each group of experimental points represented for the same CE are not coplanar, because during compaction only the CE and MC of the soil can be controlled, but the DD and consequently, void ratio (e) are results. This is consistent with previous research, in which a strong correlation between modulus and density is not observed [51,52]. However, the present study shows that if the experimental points are plotted in a MC – DD – E_{mPLT2} '3D-space', relations can be observed when sections at constant MC are taken (see next section).

As expected, the lower the CE the bigger the strain moduli k-ratio ($k = E_{mPLT2} / E_{mPLT1}$) (Fig. 5f). This is caused by a "hardening effect" during the loading process, which becomes more relevant for lower CE as specimens are more sensitive to re-compaction under the same stress level.

Correlations between k-ratio vs. MC and vs. DD apparently show a minimum value for certain state conditions. (Fig. 5g and h). The minimum k-ratio seems to be located closer to the OMC at each CE.

There are substantial differences in terms of settlement for different CE during the first loading cycle due to the sensitivity to the level of stress. However, these differences decrease in the second loading cycle. The lower the CE the sharper the difference, especially for CE = 25 % (Fig. 5i and 5j).

The empirical relationships between E_{mPLT2} and the soil state variables in a constant interval are also shown in Fig. A3 (Appendix 4). As already explained, due to the coupling between the state properties,

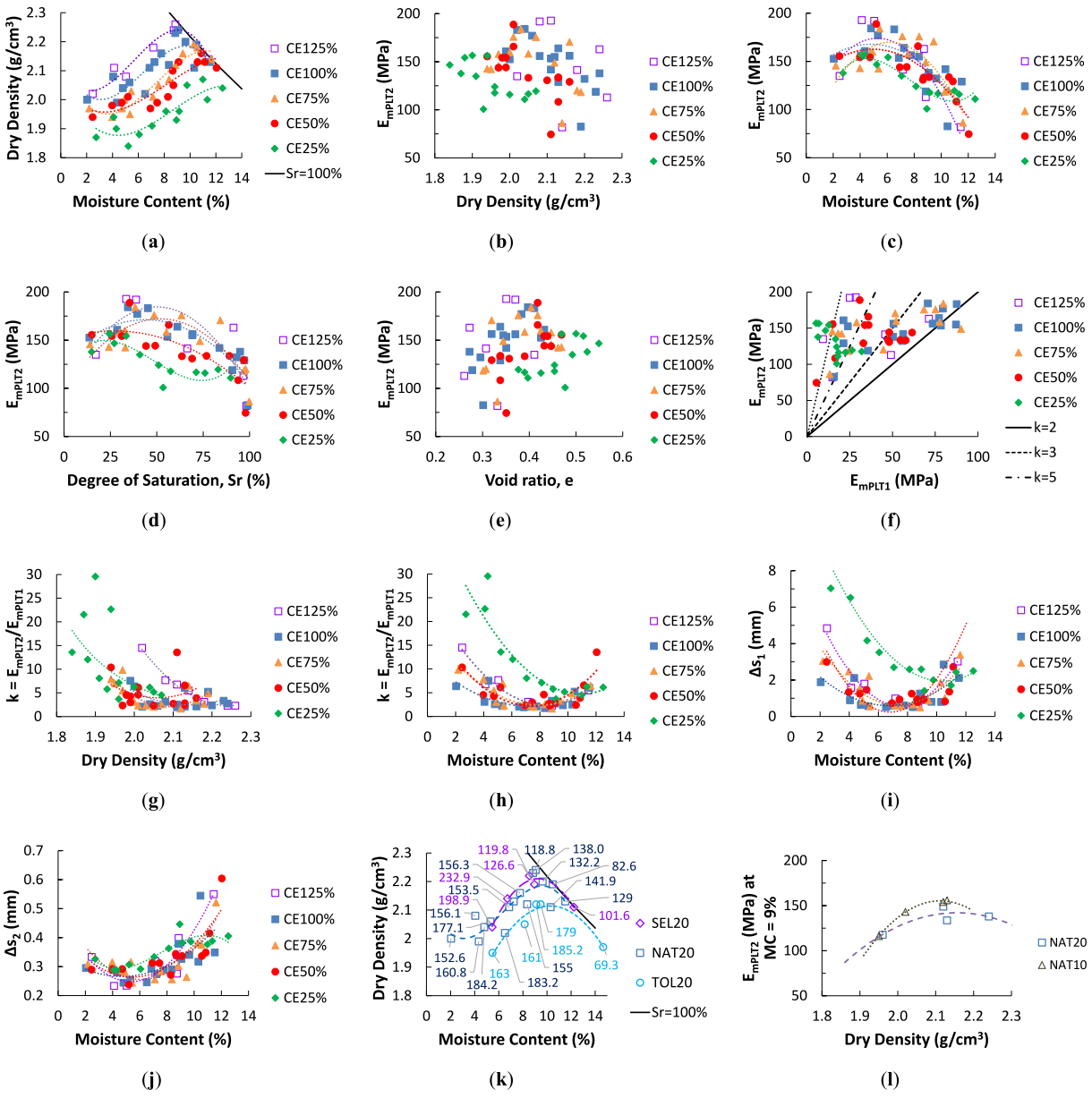

Fig. 5. Experimental relations between the soil characteristics for various compaction energies: (a) Moisture content vs. Dry density; (b) Second loading cycle strain modulus vs. Dry density; (c) Second loading cycle strain modulus vs. Moisture content; (d) Second loading cycle strain modulus vs. Degree of saturation; (e) Second loading cycle strain modulus vs. Void ratio; (f) Second loading cycle strain modulus vs. First loading cycle strain modulus; (g) Strain modulus ratio vs. Dry density; (h) Strain modulus ratio vs. Moisture content; (i) Second loading cycle strain modulus vs. settlement increment; (j) First loading cycle strain modulus vs. settlement increment; (k) Dry density – Moisture content – Strain modulus (different gradations); (l) Second loading cycle strain modulus vs. Dry density (gradation NAT20 vs. NAT 10 comparison).

which makes that the plotted points are non-coplanar, it was also not possible to determine adequate fittings in these representations, which can be determined when plotting them in a three-dimensional space (see next section).

The effect of soil gradation is shown in Fig. 5k and 5 l. In Fig. 5k, the numbers indicate the second loading cycle strain modulus (E_{mPLT2}) in MPa for each (MC – DD) point. Soil gradation referenced as "SEL" represents a high-quality gradation (i.e. well graded and small amount of low plasticity fines) based on the Spanish specifications, whereas "TOL" is a low-quality gradation. It is observed that a more selected gradation increases the maximum modulus. However, at MC near the optimum this trend is inverted (Fig. 5k). Moreover, a lower maximum particle size slightly increases the maximum modulus, contrary to reported by Ref. [53], but this stiffness is more critical to MC variation (Fig. 5l). Nevertheless, it should be noted that the effect of gradation on the stiffness also varies with the CE [54].

Geometrical interpretation: mPLT surfaces

The relations between the different parameters are represented in three-dimensional spaces using polynomial regression for soil gradation NAT20. Laboratory strain modulus (E_{mPLT2}) is plotted as a function of MC and DD generating a surface embedded in a 3D-space, to capture its dependency on both state properties (MC and DD), which cannot be decoupled due to the existence of interactions between them. For a given soil, the E_{mPLT2} surface provides the values of the strain modulus for all possible MC-DD combinations within a domain. This surface is bounded by a vertical plane passing through the higher DD that was obtained in the laboratory for this soil and by the vertical surface representing the zero-air void line ($S_r = 100$ %). Note that unlike the zero-air void, which

is a physical limit, the maximum experimental DD boundary defined is only a practical limit. This could be extended to the plane corresponding to the maximum DD that minimises the void ratio, which does constitute a physical limit (i.e. any MC – DD point located beyond this plane would imply a change in soil gradation).

The E_{mPLT2} surface is plotted in Fig. 6a ($R^2 = 0.63$) and its related contour plot is shown in Fig. 6b. As it can be seen, strain modulus seems to increase towards the source of all the isosaturation lines, which represents the maximum theoretical DD (i.e. at MC = 0 and e = 0). At a fixed S_r, the stiffness raises with increasing DD, similar to the results observed for the shear modulus by Ref. [55]. In the present study, the strain modulus shows a relative maximum with MC variation for a constant DD.

At the theoretical point of absolute maximum DD, the soil —understood as a 3-phase system— becomes an ideal solid without any voids. In practice, this situation is not physically possible because reaching extremely high DD with extremely low MC would imply increasing the compaction energy (CE) to disproportionately high levels, making the process rather inefficient as well as causing a significant change in the soil structure (i.e. fracture of solid particles).

The E_{mPLT2} surface provides, for a given soil and a specific CE, the combinations of MC – DD values that offer the maximum strain modulus. As can be seen in Fig. 6b, the maximum strain modulus does not coincide with the point of maximum dry density (MDD) and optimum moisture content (OMC) for each CE. The highest moduli tend to be located on the dry side of the MP curve. Fig. 6c shows that for a constant DD, the modulus presents a relative maximum for a certain MC. The same applies to the saturation ratio (S_r) (Fig. 6e). However, for a constant MC the variation trend of the modulus with the DD depends on the moisture content (Fig. 6d), so that only when S_r is constant the modulus is increasing with DD (Fig. 6f).

Fig. 7a shows a general view of the polynomial regression model for the k-ratio = E_{mPLT2} / E_{mPLT1} ($R^2 = 0.57$). The surface is bounded by the same limits as the E_{mPLT2} surface. For each CE, the minimum k-ratio value tends to be in a region closer to the line of optimums (the line connecting MDD – OMC points for increasing CE) as observed in Fig. 7b. This stands to logic, since the higher DD the more likely it is that the modulus of the first loading cycle will be closer to that obtained in the second cycle. This trend can also be seen in the corresponding cross-sections Fig. 7c and d (i.e. cutting planes at DD = constant or MC = constant, respectively).

As observed, the maximum moduli are located on the dry side of the MP compaction curves. However, soils compacted to low MC can be susceptible to collapse settlements. This confirms the need of simultaneously fulfil requirements in terms of sufficient modulus, limited k-ratio, and MDD – OMC conditions for field compaction quality control

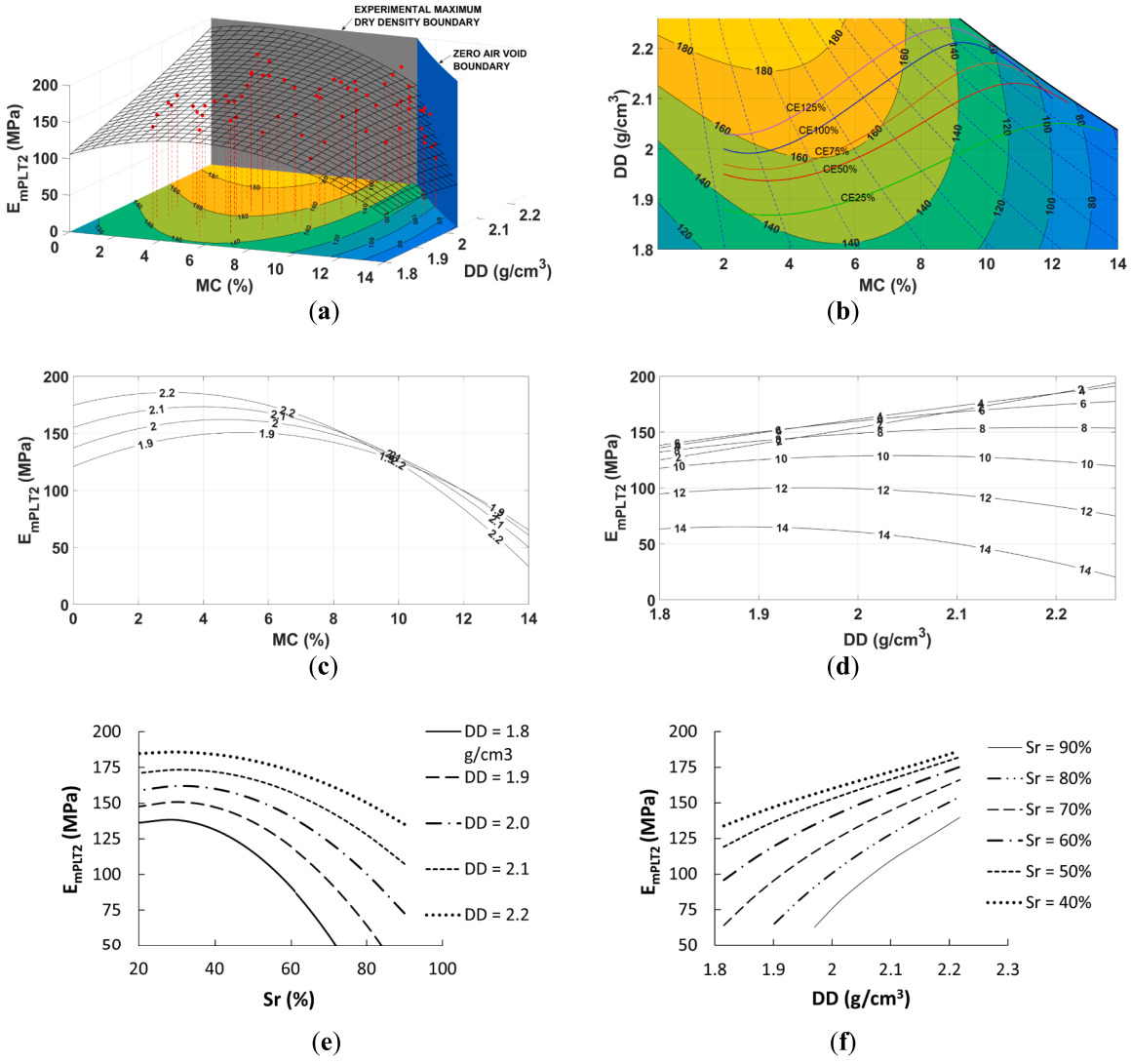

Fig. 6. Moisture Content – Dry Density – Strain Modulus '3D-space': (a) E_{mPLT2} surface and boundaries; (b) E_{mPLT2} surface contour lines on the MC – DD plane; (c) E_{mPLT2} surface sections at constant DD; (d) E_{mPLT2} surface sections at constant MC; (e) E_{mPLT2} vs. Saturation ratio (S_r) at constant DD; (f) E_{mPLT2} vs. DD at constant S_r.

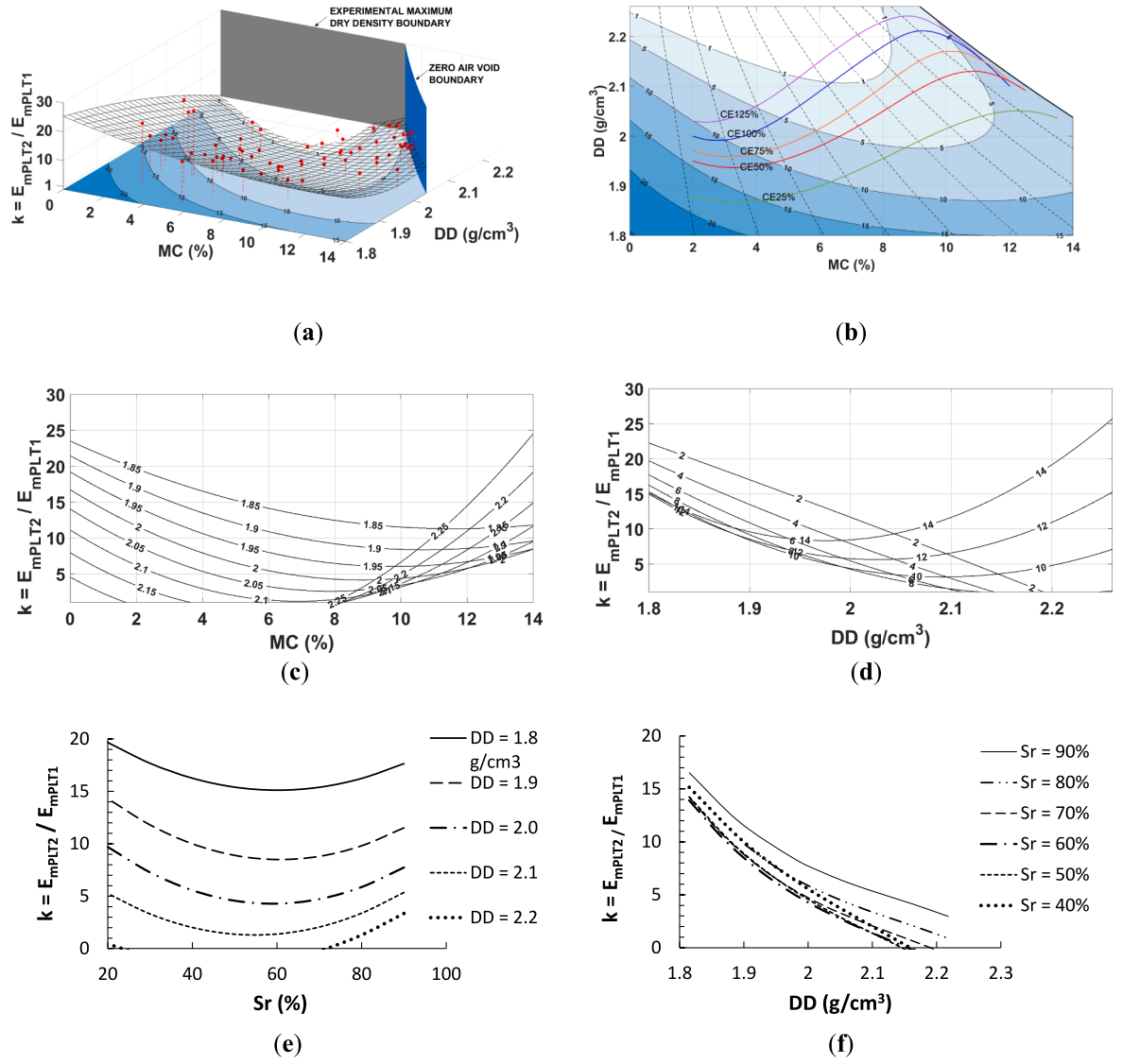

Fig. 7. Moisture Content – Dry Density – k-ratio '3D-space'. (a) k-ratio surface and boundaries; (b) k-ratio surface contour lines on the MC – DD plane; (c) k-ratio surface sections at constant DD; (d) k-ratio surface sections at constant MC; (e) k-ratio vs. saturation ratio (S_r) at constant DD; (f) k-ratio vs. DD at constant S_r.

specifications.

Correlation between laboratory strain modulus and field strain modulus

A set of field static plate load test were conducted on a road embankment built using the same material (i.e. NAT20 gradation but with particles up to 100 mm in size). Field moisture content and dry density were measured. Fig. 8 presents the results of the empirical correlation between the second loading cycle strain modulus (E_{v2}) obtained in the field using static plate load test (300 mm in diameter) and the second loading cycle strain modulus (E_{mPLT2}) obtained in the laboratory test, for the same moisture and density conditions previously measured in the field. This last correction was possible by using the analytical expression of the E_{mPLT2} surface.

The correlation between the static field PLT strain modulus and the laboratory mPLT strain modulus fits well with a linear model, being the values of the latter slightly greater than the values of the former. In this case, the confinement effect of the mPLT mould, which has an influence on the magnitude of the related settlement, is partially compensated due to the use of Boussinesq's formulation for the half-space (unconfined situation) in the calculation process of the experimental mPLT modulus,

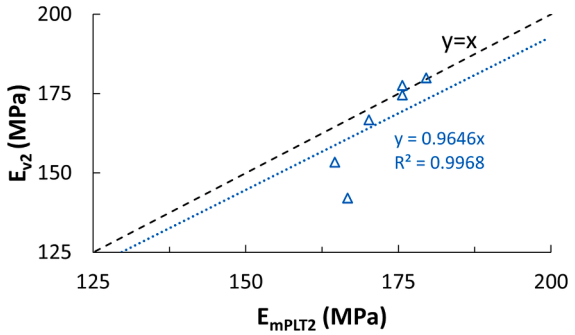

Fig. 8. Correlation between laboratory mPLT modulus (E_{mPLT2}) and field PLT modulus (E_{v2}).

which physically corresponds to a confined situation.

Practical application of this method

At the design stage of embankments, subgrades, and granular bases

and subbases of pavements, the following procedure to estimate the elastic modulus of a certain compacted granular geomaterial required for analytical and computational design is suggested:

1. Perform a Modified Proctor (MP) test, as specified in the technical standards, for each type of soil to be used in the embankments or granular layers of the pavement.
2. Conduct a mPLT immediately after the compaction of each MP laboratory specimen following the loading scheme described in section "Materials and laboratory testing". The preloading and the maximum applied force should be adjusted depending on the soil type and CBR value. As a result of the mPLT, the strain modulus corresponding to each pair of dry density (DD) – moisture content (MC) values will be known.
3. Obtain the range of foreseeable values of the E_{mPLT2} modulus within the validity zone (i.e. target area according to specifications of the set of DD – MC values, Fig. 9a). As design modulus, select the one considered more suitable from those in the validity zone, depending on the quality-control level during construction and the factor of safety specified by the design codes. The designer may consider possible changes in the soil moisture content during the service life of the infrastructure. It must also be verified that the soil state conditions (DD – MC values) that correspond to the selected modulus provide a k-ratio (Fig. 9b) that does not exceed the maximum limit of the technical specifications for this type of compacted fill.
4. Convert this laboratory strain modulus (E_{mPLT2}) into an elastic modulus for use in analytical design (i.e. multilayered elastic model) by using Fig. 10. As an alternative, the analytical expression given by Eq. (4) can be used. This Young's modulus needs to be consistent with the Poisson's coefficient assigned in design.

The mPLT may also be used as a reference test to meet compaction quality control requirements during the construction phase, by providing an optimum MC range within which strain modulus (Fig. 9a), k-ratio (Fig. 9b) and DD requirements are satisfied.

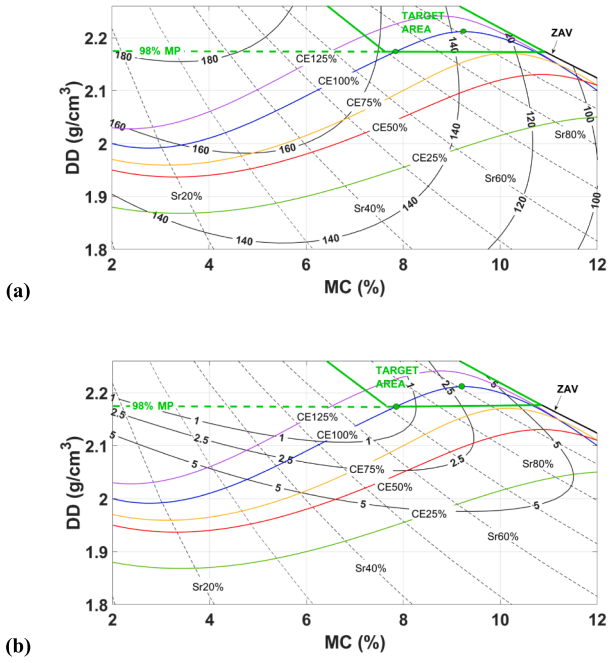

Fig. 9. Practical application of the relations obtained through mPLT test: (a) Estimation of the E_{mPLT2} modulus within the (MC – DD) region bounded by the technical specifications; (b) Verification of the k-ratio within the same region. (Note: CEX% is the compaction curve corresponding to a compaction energy level of X% with respect to the energy specified for a MP compaction test. SrX% is the isoline corresponding to X% of saturation).

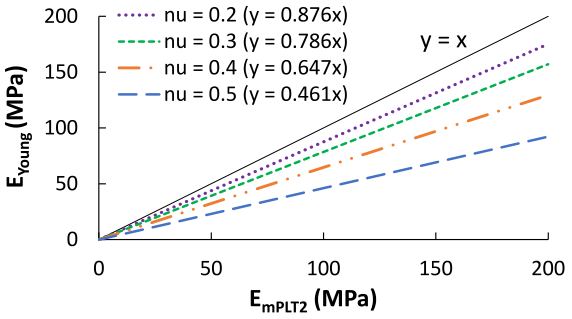

Fig. 10. Estimation of Young's modulus for use in analytical design from the experimental E_{mPLT2} modulus for various Poisson's ratios (ν).

Conclusions

Based on the experimental results and on the 'miniature plate load test' (mPLT) surfaces presented in this study, the following conclusions may be drawn:

- The second loading cycle strain modulus increases towards the point that represents the maximum theoretical dry density, where all the isosaturation lines converge.
- For a constant dry density, the modulus presents a relative maximum for a certain moisture content, whereas for a constant moisture content the variation trend of the modulus with the dry density depends on such moisture content. When the moisture content is low, the soil is further away from full saturation and therefore an increase in dry density is also reflected in an increase in stiffness; on the contrary, with high moisture contents, above certain dry densities the stiffness decreases with increasing the dry density, as the soil conditions are closer to saturation. Only if the saturation ratio is constant the modulus is increasing with the dry density.
- For a given soil and compaction energy, there is a combination of moisture content – dry density that maximises the strain modulus. This point does not coincide with the point of maximum dry density (with optimum moisture content) of the related Modified Proctor (MP) compaction curve, being located on its dry side.
- Similarly, for a given soil and compaction energy, there is also a combination of state conditions (moisture content – dry density) that minimises the k-ratio. This minimum k-ratio also seems to be on the dry side but closer to the maximum dry density for each MP compaction curve.
- The proposed procedure predicts the strain modulus of compacted granular fills, by means of a low-cost and easy-to-conduct laboratory test that uses simple and well-known equipment. This test correctly captures the effect of any variation in the soil state conditions on the soil stiffness.
- The applied numerical model allows to correlate the experimental laboratory strain modulus with the Young's modulus needed for analytical design considering the differences in geometry and boundary conditions between the proposed laboratory test and the standard in situ test.
- Since the three properties of the compacted soil are obtained in the same test, the relationship between the state properties (moisture and dry density) and the expected strain modulus can be determined using this method, which makes it possible to optimize the analytical design and thus, contributing to improve the quality and reduce costs and environmental impacts.
- For field compaction quality control, the analysis of the second loading cycle strain modulus and k-ratio surfaces experimentally confirmed the need of simultaneously fulfil requirements in terms of sufficient stiffness, limited k-ratio, and maximum dry density –

optimum moisture conditions. The mPLT procedure could also be used during the construction phase as a reference test to ensure this is met by providing an optimum moisture content range within which, strain modulus, k-ratio and dry density requirements are satisfied.

This new methodology, that we propose to name '**Canarian mPLT**', is not intended to be a substitute for on-site full-scale field plate load tests or laboratory cyclic triaxial tests, but a complementary and cost-effective tool to assist in the design process and during construction. For practical applications, it is recommended to apply this test to compacted specimens at energy levels and state conditions (moisture content and dry density) in which the loads applied do not cause excessive deformations, as specified in the PLT standards. For this reason, an adjustment to the maximum applied stress is suggested in this study.

As further research, it is suggested extending this study to other soil types to confirm whether the proposed surfaces maintain the observed global trends. A comparison between the results obtained with this new laboratory test and the cyclic triaxial tests is of interest. The study of the variation of the modulus with time and the implementation of non-destructive methods to monitor moisture content would also be of great practical interest. It is also suggested to explore the influence of soil microstructure on stiffness. In addition to this, the research on numerical models that consider important aspects such as non-uniformity, anisotropy and non-linearities would be interesting to explore. In this sense, a more comprehensive study on the influence of different parameters (e.g. boundary conditions, loading) would also be beneficial.

Data Availability Statement

Data will be made available on request.

CRediT authorship contribution statement

Samuel Valencia-Díaz: Writing – review & editing, Writing – original draft, Visualization, Validation, Software, Methodology, Investigation, Formal analysis, Data curation, Conceptualization. **Jacob D.R. Bordón:** Writing – review & editing, Supervision, Software, Data curation, Conceptualization. **J. Yepes:** Supervision, Methodology. **Juan J. Aznárez:** Writing – review & editing, Supervision, Software. **Miguel A. Franesqui:** Writing – review & editing, Writing – original draft, Visualization, Validation, Supervision, Resources, Project administration, Methodology, Investigation, Funding acquisition, Formal analysis, Data curation, Conceptualization.

Funding

This work was funded by the Regional Government of the Canary Islands (Spain), through the research project: "Technical regulations for the design and construction of road pavements in the road network of the Canary Islands" (Agreement C2020/143, "Convenio de cooperación con la Consejería de Obras Públicas, Transportes y Vivienda para la elaboración de la Guía de recomendaciones técnicas para el diseño y ejecución de firmes en la red de carreteras de Canarias"). The APC was supported by the same funder.

Declaration of competing interest

The authors declare that they have no known competing financial interests or personal relationships that could have appeared to influence the work reported in this paper.

Appendix 1. . Materials

.

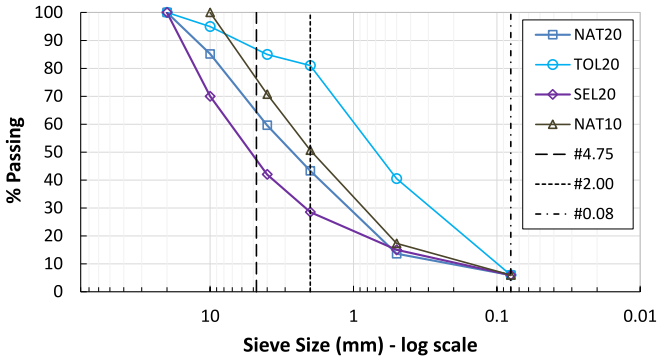

Fig. A1. Grading curves of the different soil gradations tested in this research.

.

Appendix 2. . Numerical model

.

Table A1
Average stress below the loaded area for an imposed unit settlement (1 mm) and a reference Young's modulus of 50 MPa (Frictionless mould side wall).

Poisson's ratio, ν	Average stress, Δσ (MPa)	(E*1mm) / (Δσ * r)
0.10	1.4485	1.3807
0.15	1.4779	1.3533
0.20	1.5237	1.3126

(*continued on next page*)

Table A1 (*continued*)

Poisson's ratio, ν	Average stress, Δσ (MPa)	(E*1mm) / (Δσ * r)
0.25	1.5915	1.2567
0.30	1.6902	1.2833
0.35	1.8359	1.0894
0.40	2.0600	0.9709
0.45	2.4327	0.8221
0.50	3.1474	0.6354

.

Table A.1.2
Comparison between settlements of a rigid plate for friction and frictionless mould side wall based on a reference Young's modulus of 50 MPa.

Poisson's ratio, ν	Δs (mm) (Frictionless side wall)	Δs (mm) (Friction side wall)	Difference (%)
0.20	0.7875	0.6933	11.97
0.25	0.7540	0.6739	10.62
0.30	0.7100	0.6475	8.80
0.35	0.6536	0.6118	6.40
0.40	0.5825	0.5620	3.51
0.45	0.4933	0.4850	1.67

Appendix 3. . Statistical analysis

.

Table A2
Main statistics of laboratory tests for NAT20 soil gradation.

Variable	CE	N	Median	Mean	SEM	SD	CV	MAD	S-W	p-value
MC (%)	125	7	7.16	6.83	1.18	3.13	0.46	2.12	0.971	0.905
	100	16	7.50	7.32	0.67	2.67	0.37	2.17	0.975	0.91
	75	14	7.34	7.17	0.75	2.81	0.39	2.27	0.967	0.832
	50	14	8.47	7.86	0.78	2.91	0.37	2.25	0.957	0.675
	25	13	8.13	7.71	0.85	3.08	0.40	2.85	0.965	0.83
DD (g/cm^3)	125	7	2.14	2.15	0.03	0.09	0.04	0.06	0.97	0.902
	100	16	2.12	2.11	0.02	0.08	0.04	0.07	0.962	0.699
	75	14	2.04	2.06	0.02	0.09	0.04	0.08	0.92	0.217
	50	14	2.03	2.05	0.02	0.07	0.04	0.07	0.9	0.112
	25	13	1.94	1.95	0.02	0.07	0.04	0.06	0.956	0.699
S_r (%)	125	7	66.40	63.17	12.69	33.56	0.53	30.32	0.881	0.229
	100	16	65.12	62.90	7.08	28.32	0.45	26.77	0.923	0.189
	75	14	51.89	56.57	7.90	29.57	0.52	21.54	0.918	0.204
	50	14	60.01	60.29	7.48	27.99	0.46	26.75	0.941	0.433
	25	13	51.03	49.82	6.83	24.62	0.49	23.93	0.943	0.501
e	125	7	0.33	0.33	0.02	0.05	0.16	0.04	0.969	0.89
	100	16	0.35	0.35	0.01	0.05	0.14	0.04	0.956	0.596
	75	14	0.40	0.39	0.02	0.06	0.15	0.06	0.917	0.201
	50	14	0.41	0.39	0.01	0.05	0.13	0.05	0.907	0.141
	25	13	0.47	0.46	0.02	0.05	0.12	0.04	0.963	0.797
E_{mPLT1} (MPa)	125	7	28.50	34.83	8.22	21.75	0.62	17.20	0.95	0.729
	100	16	56.00	55.31	6.30	25.18	0.46	21.75	0.904	0.093
	75	14	48.15	47.11	7.32	27.37	0.58	27.45	0.902	0.122
	50	14	35.95	37.44	4.49	16.78	0.45	12.15	0.95	0.56
	25	13	17.40	16.24	2.19	7.89	0.49	5.10	0.95	0.6
E_{mPLT2} (MPa)	125	7	141.40	145.54	15.40	40.73	0.28	28.50	0.947	0.703
	100	16	154.25	149.08	6.43	25.70	0.17	14.30	0.927	0.216
	75	14	153.50	149.06	7.12	26.62	0.18	14.15	0.927	0.276
	50	14	138.80	139.30	7.16	26.80	0.19	12.50	0.934	0.347
	25	13	124.10	130.18	5.22	18.83	0.15	13.20	0.919	0.24

(*continued on next page*)

Table A2 (*continued*)

Variable	CE	N	Median	Mean	SEM	SD	CV	MAD	S-W	p-value
$k = E_{mPLT2} / E_{mPLT1}$	125	7	5.49	6.02	1.63	4.32	0.72	2.40	0.851	0.125
	100	16	2.57	3.39	0.46	1.84	0.54	0.50	0.774	0.001
	75	14	3.19	4.39	0.68	2.56	0.58	1.34	0.881	0.06
	50	14	4.11	4.97	0.89	3.31	0.67	1.53	0.78	0.003
	25	13	7.13	11.25	2.30	8.29	0.74	2.60	0.815	0.01
Δs_1 (mm)	125	7	1.58	1.97	0.57	1.49	0.76	0.66	0.85	0.124
	100	16	0.81	1.10	0.18	0.73	0.66	0.24	0.778	0.001
	75	14	0.94	1.44	0.27	0.99	0.69	0.41	0.852	0.024
	50	14	1.25	1.84	0.52	1.95	1.06	0.31	0.566	< 0.001
	25	13	2.59	3.67	0.63	2.25	0.62	0.89	0.821	0.012
Δs_2 (mm)	125	7	0.32	0.33	0.04	0.11	0.34	0.08	0.878	0.219
	100	16	0.29	0.31	0.02	0.07	0.23	0.04	0.767	0.001
	75	14	0.29	0.31	0.02	0.07	0.23	0.03	0.795	0.004
	50	14	0.33	0.34	0.02	0.09	0.26	0.03	0.751	0.001
	25	13	0.36	0.35	0.01	0.05	0.15	0.03	0.929	0.329

(CE) Compaction energy as percent relative to Modified Proctor test; (N) Sample size; (SEM) Standard error of mean; (SD) Standard deviation; (CV) Coefficient of variation; (MAD) Mean absolute value; (S-W): Shapiro-Wilk normality test; (MC) Moisture content; (DD) Dry density; (S_r) Saturation ratio; (e) Void ratio; (E_{mPLT1}) First loading cycle secant strain modulus from mPLT; (E_{mPLT2}) Second loading cycle secant strain modulus from mPLT; (Δs_1) First loading cycle settlement increment; (Δs_2) Second loading cycle settlement increment.

Fig. A2 shows the variation of the variables of interest between groups of soil specimens prepared at same CE. MC was taken as a controlled parameter so little overall variation between groups exists (Fig. A2a). As expected, the DD clearly decreases together with the CE, although the difference between 75 % and 50 % groups was relatively low (Fig. A2b). The void ratio (e) also shows a clear pattern, increasing with a decrease in CE (Fig. A2c). The saturation ratio (S_r) trend responds to the theoretical relationship between MC and void ratio (Fig. A2d). The first cycle strain modulus (E_{mPLT1}) decreases as the CE decreases (Fig. A2e). The second cycle strain modulus (E_{mPLT2}) does not show a constant trend, with low difference between 100 % and 75 % groups (Fig. A2f). The moduli k-ratio presents a high difference between the 25 % group and the rest as it is much more susceptible to the level of stress applied (Fig. A2g). The same may be stated for the settlement increment during the first loading cycle (Δs_1) vs. the CE. It can be deduced that when the degree of compaction is lower, the sample exhibits a large plastic deformation at the first loading cycle (Fig. A2h). The settlement increment in the second loading cycle (Δs_2) also tends to increase as CE decreases, but this trend is much less abrupt (Fig. A2i).

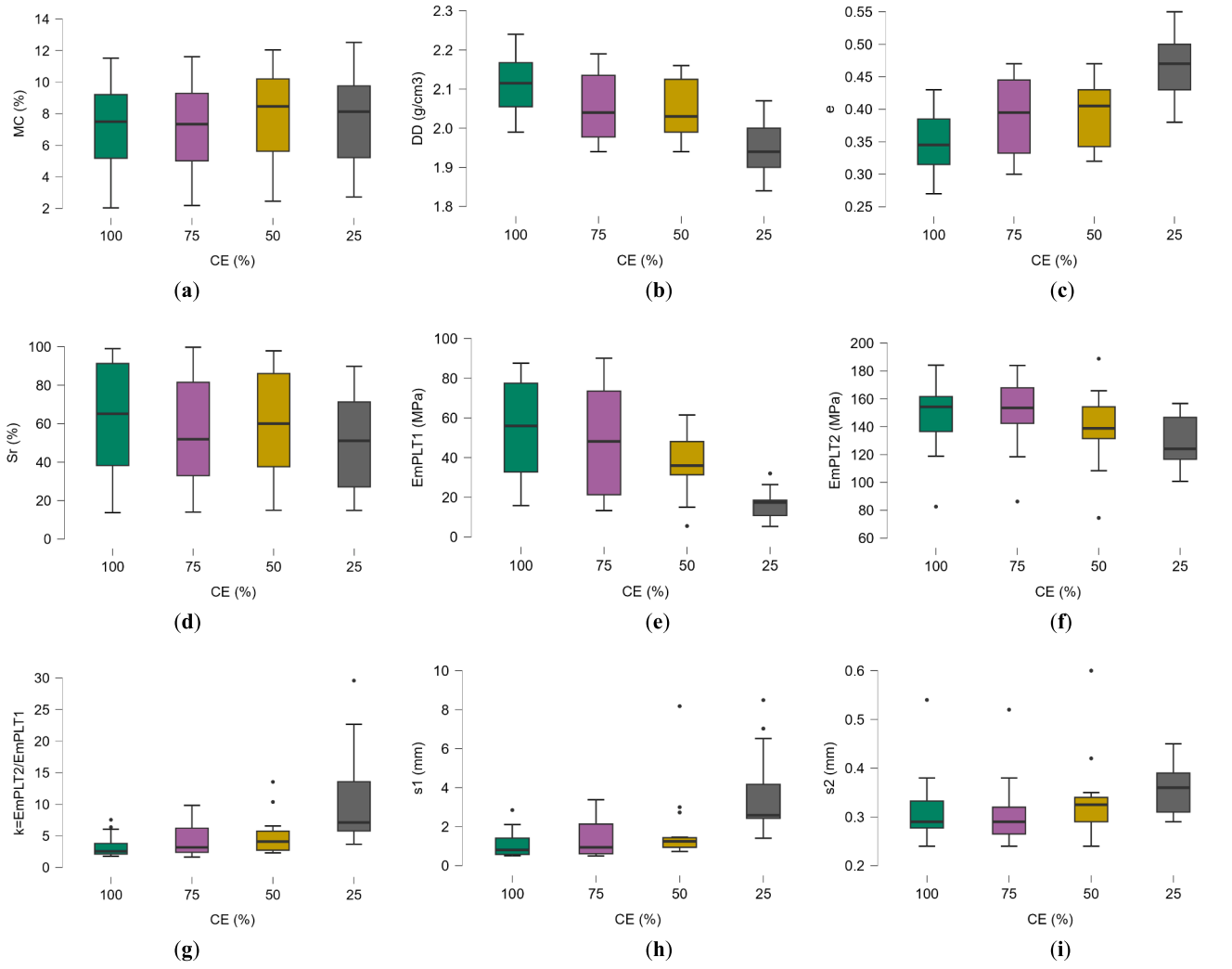

Fig. A2. Box and whisker plots of soil characteristics grouped by compaction energy (CE), expressed as a percent relative to Modified Proctor test [Note that 125 % value is excluded due to the small sample size]: (a) Moisture Content (MC); (b) Dry Density (DD); (c) Void Ratio (e); (d) Saturation ratio (S_r); (e) 1st loading cycle strain modulus (E_{mPLT1}); (f) 2nd loading cycle strain modulus (E_{mPLT2}); (g) Moduli k-ratio; (h) First loading cycle settlement (Δs_1); (i) Second loading cycle settlement (Δs_2).

.

Appendix 4. . Relations between stiffness and state properties

.

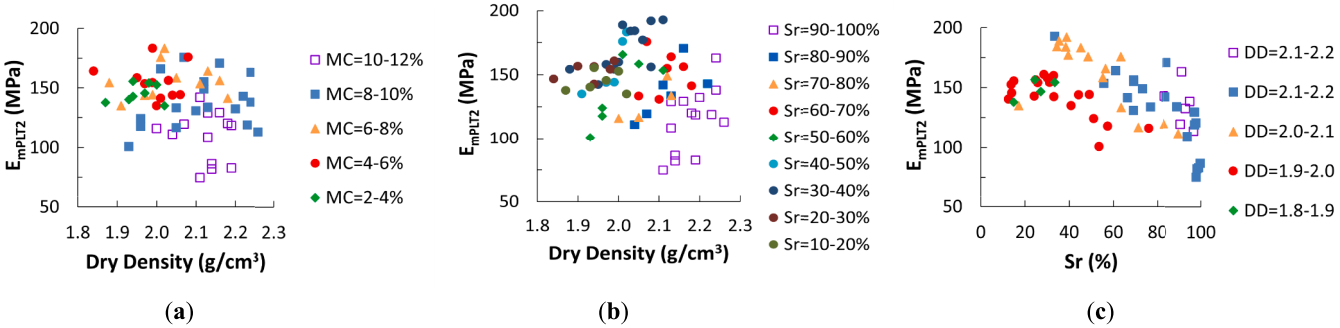

Fig. A3. Experimental relations between the second loading cycle strain modulus (E_{mPLT2}) and the soil state properties (DD, MC and S_r) in a constant interval.

.

Data availability

Data will be made available on request.

References

[1] Novakov, A. (2023). Report on large transport infrastructure projects in the EU – implementation of projects and monitoring and control of EU funds. European Parliament: Report - A9-0181/2023. https://www.europarl.europa.eu/doceo/document/A-9-2023-0181_EN.html.

[2] Monismith, C. L. (2004). Evolution of long-lasting asphalt pavement design methodology: a perspective. In ISAP International Symposium on Design and Construction of Long-Lasting Asphalt Pavements. June (pp. 7-9).

[3] Papagiannakis AT, Masad EA. Pavement design and materials. John Wiley & Sons; 2008.

[4] Farzin MH, Krizek RJ, Corotis RB. Evaluation of modulus and poisson's ratio from triaxial tests. Transp Res Rec 1975;537:69–80.

[5] AASHTO (2015). Mechanistic-Empirical Pavement Design Guide (MEPDG): A Manual of Practice. 2nd Edition. ISBN 10: 156051597X / ISBN 13: 9781560515975.

[6] Elliott, R. P., & Thornton, S. I. (1988). Resilient modulus and AASHTO pavement design. Transportation research record, (1196).

[7] Kim D, Siddiki NZ. Simplification of resilient modulus testing for subgrades. Joint transportation. Res Program 2006;265.

[8] Porter, O. J. (1943). Foundations for flexible pavements. In Highway Research Board Proceedings (Vol. 22).

[9] Proctor R. Fundamental principles of soil compaction. Eng News-Rec 1933;111 (13).

[10] Hogentogler CA. Essentials of soil compaction In Proceedings of the Highway Research Board. Washington, DC: National Research Council; 1936. p. 309–16.

[11] Hamilton, L. W., Preece, E. F., Stanton, T. E., Johnson, A. W., Woods, K. B., Casagrande, L., & Allen, H. (1939). Compaction of earth embankments. In: Highway Research Board Proceedings (Vol. 18).

[12] Xu G, Chang GK, Wang D, Correia AG, Nazarian S. The pioneer of intelligent construction—an overview of the development of intelligent compaction. J Road Eng 2022;2(4):348–56.

[13] Nazarian S, Mazari M, Abdallah IN, Puppala AJ, Mohammad LN, Abu-Farsakh MY. Modulus-based construction specification for compaction of earthwork and unbound aggregate. Washington, DC: Transportation Research Board; 2015.

[14] Schwartz, C. W., Afsharikia, Z., & Khosravifar, S. (2017). Standardizing lightweight deflectometer modulus measurements for compaction quality assurance (No. MD-17-SHA-UM-3-20). Maryland. State Highway Administration.orter, O. J. (1943). Foundations for flexible pavements. In Highway Research Board Proceedings (Vol. 22).

[15] Tatsuoka F, Correia AG. Importance of controlling the degree of saturation in soil compaction linked to soil structure design. Transp Geotech 2018;17:3–23.

[16] Tatsuoka F, Hashimoto T, Tateyama K. Soil stiffness as a function of dry density and the degree of saturation for compaction control. Soils Found 2021;61: 989–1002.

[17] Briaud JL. Introduction to soil moduli. Geotech News 2000;19(2):54–8.

[18] Middlebrooks TA, Bertram GE. Soil tests for design of runway pavements. Highway Res Board 1942.

[19] Foster, C. R., & Ahlvin, R. G. (1954). Stresses and deflections induced by a uniform circular load. In: Highway Research Board Proceedings (Vol. 33).

[20] American Society for Testing Materiales, ASTM (2004). D1195/D1195M-21. Standard Test Method for Repetitive Static Plate Tests of Soils and Flexible Pavement Components for Use in Evaluation and Design of Airport and Highway Pavements.

[21] Asociación Española de Normalización, AENOR (2006). UNE. Ensayo de carga vertical de suelos mediante placa.

[22] Deutches Institut für Normung, DIN (2012). DIN 18134. Plate load test. English translation of DIN 18134:2012-04.

[23] Han HCS, Hirst TJ, Fang HY. Determination of the elastic moduli of flexible pavement components. Highw Res Rec 1972;407:36–8.

[24] Heukelom W, Foster CR. Dynamics testing of pavements. J Soil Mech Foundations Div 1960;86(1):1–28.

[25] Heukelom, W., & Klomp, A. (1962). Dynamic testing as a means of controlling pavements during and after construction. In: International Conference on the Structural Design of Asphalt PavementsUniversity of Michigan, Ann Arbor (Vol. 203, No. 1).

[26] Powell, W. D., Potter, J. F., Mayhew, H. C., Nunn, M. E., Design, P., & Crowthorne, B. (1983). TRRL Laboratory Report 1132.

[27] Brown SF, O'Reilly MP, Loach SC. The relationship between California Bearing Ratio and elastic stiffness for compacted clays. Ground Eng 1990;23(8).

[28] Deng, M., Wang, J., Wang, X., Xie, X., Kaiwei Wang, K. & He, Y. (20024). Research on correlation between dynamic resilient modulus and CBR of coarse-grained chlorine saline soil. Scientific Rep, 14, 4854.

[29] Federal Aviation Administration [U.S. Department of Transportation] (2021). Airport Pavement Design and Evaluation. Advisory Circular AC No: 150/5320-6G.

[30] Sukumaran, B., Kyatham, V., Shah, A., & Sheth, D. (2004). Suitability of using California Bearing Ratio test to predict resilient modulus. In Proceedings: Federal Aviation Administration Airport Technology Transfer Conference (p. 9).

[31] Putri EE, Rao NSVK, Mannan MA. Evaluation of modulus of elasticity and modulus of subgrade reaction of soils using CBR test. J Civ Eng Res 2012;2(1):34–40.

[32] Hajiannia A, Dorobati MT, Kasaeian S, Baghbadorani SB. Correlation between the results of the PLT and CBR tests to determine the elasticity modulus. Australian Geomechanics Society; 2017. p. 701–6.

[33] Narzary, B. K., & Ahamad, K. U. (2018). Estimating elastic modulus of California bearing ratio test sample using finite element model.

[34] Morais, H., Minhoto, M., & Paula, A. M. (2018). Relação entre módulo de deformabilidade e CBR para caracterização mecânica da fundação de pavimentos. In 16°Congresso Nacional de Geotecnia.

[35] Plati C, Tsakoumaki M. A critical comparison of correlations for rapid estimation of subgrade stiffness in pavement design and construction. Constr Mater 2023;3(1): 127–42.

[36] Abed, Y., & Kaddouri, A. (2024). Elastic modulus-CBR Index correlation using FEM. 18th African Regional Conference on Soil Mechanics and Geotechnical Engineering.

[37] Oh WT, Vanapalli SK. Scale effect of plate load tests in unsaturated soils. Geomate J 2013;4(8):585–94.

[38] Hyuk J, Hwan Y, Jin K, Min S. Field verification of small loading plate for laboratory cyclic plate loading test. J Korean Soc Railway 2018;21(6):578–92.

[39] Son M, Jung HS, Yoon HH, Sung D, Kim JS. Numerical study on scale Effect of repetitive plate-loading test. Appl Sci 2019;9(20):4442.

[40] Wang J, Birgisson B. A time domain boundary element method for modeling the quasi-static viscoelastic behavior of asphalt pavements. Eng Anal Bound Elem 2007;31(3):226–40.

[41] Brebbia CA. The boundary element method in engineering practice. Eng Anal 1984;1:3–12.

[42] Pak RYS, Guzina BB. Three-dimensional Green's functions for a multilayered half-space in displacement potentials. J Eng Mech 2002;128(4):449–61.

[43] García-González C, Yepes J, Franesqui MA. Geomechanical characterization of volcanic aggregates for paving construction applications and correlation with the rock properties. Transp Geotech 2020;24:100383.

[44] Spanish Ministry of Infrastructures (2002). Spanish General Technical Specifications for Roads and Bridges (PG-3, Art. 330). Orden FOM/1382/2002. Madrid, Spain (in Spanish).

[45] Pacheco LG, Nazarian S. Impact of moisture content and density on stiffness-based acceptance of geomaterials. Transp Res Rec 2011;2212(1):1–13.

[46] Adam C, Adam D, Kopf F, Paulmichl I. Computational validation of static and dynamic plate load testing. Acta Geotech 2009;4:35–55.

[47] Bordón JD, Álamo GM, Padrón LA, Aznárez JJ, Maeso O. MultiFEBE: a multi-domain finite element–boundary element solver for linear mixed-dimensional mechanical problems. SoftwareX 2022;20:101265.

[48] Geuzaine C, Remacle JF. Gmsh: A 3-D finite element mesh generator with built-in pre-and post-processing facilities. Int J Numer Meth Eng 2009;79(11):1309–31.

[49] Lee PY, Suedkamp RJ. Characteristics of irregularly shaped compaction curves of soils. Highw Res Rec 1972;381:1–9.

[50] Liu K, Chen WB, Feng WQ, Tan DY, Zhou C, Yin JH. Variation of Secant Young's Modulus in an Unsaturated Gap-Graded Granular Fill. Transp Geotech 2024;49: 101416.

[51] Mooney MA. Intelligent soil compaction systems. Transportation Research Board; 2010.

[52] Von Quintus HL. Evaluation of intelligent compaction technology for densification of roadway subgrades and structural layers. Wisconsin Highway. Res Program 2010.

[53] Kolisoja P. Resilient deformation characteristics of granular materials. Finland: Publications: Tampere University of Technology; 1997. p. 188–201.

[54] Thom, N. H., & Brown, S. F. (1988). The effect of grading and density on the mechanical properties of a crushed dolomitic limestone. In Australian Road Research Board (ARRB) Conference, 14th, 1988, Canberra (Vol. 14, No. 7).

[55] Latimer R, Airey D, Tatsuoka F. Expected stiffness changes during compaction in laboratory and field. Transp Geotech 2023;43:101136.